

The lability of the two chloro ligands of $\text{Mn}(\text{B14N4})\text{Cl}_2^+$ was probed by simple ligand exchange reactions. Qualitatively, several monodentate, monoanionic ligands appear to replace chloride if an excess of the anion is stirred with the complex in acetonitrile solution. To illustrate this reactivity, the bis-azido complex was

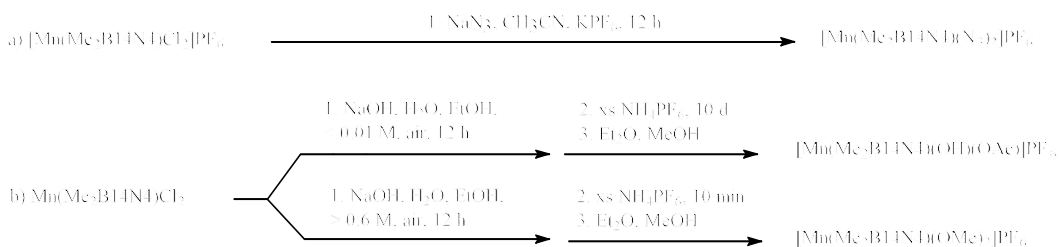


Figure 71. Synthesis of additional $\text{Mn}(\text{Me}_2\text{B14N4})^{3+}$ complexes

prepared by just such a reaction (**Figure 71a**).¹⁶⁷ The product was obtained in high (77%) yield and gave X-ray quality crystals upon ether diffusion into its methylene chloride solution. This reaction shows that the chloro ligands are relatively labile in acetonitrile solution and that the occupancy of the labile *cis* coordination sites should be easily manipulated for further studies. The bis-azido complex has similar properties to the dichloro complex (*vide infra*).

Two somewhat more compelling $\text{Mn}(\text{B14N4})^{3+}$ complexes were obtained from reactions under aqueous conditions. It is well known that synthetic manganese complexes tend to form dimeric or polymeric oxo-bridged species in oxygenated basic aqueous solutions.¹⁸³ However, Cache[®] molecular modeling studies indicated that the methyl groups protruding from the two non-bridgehead ligand nitrogens would interfere with dimerization, through formation of the common bis-(μ -oxo) diamond core structure, of the present manganese complexes. Models with this type of oxygen bridging would place the methyl groups of both ligands in approximately

the same locations in space. To test for the formation of dimers, as well as to test the stability of the complex under strongly basic conditions, $\text{Mn}(\text{B14N4})\text{Cl}_2$ was dissolved in 5:1 water:ethanol solution containing 2 M NaOH, and air was bubbled through the solution overnight. Oxidation to Mn^{3+} is seemingly very fast, as the nearly colorless starting material gives a golden brown solution almost immediately. No evidence of dimerization was found; i.e., neither the characteristic green color nor 16-line EPR spectrum¹⁸³ associated with the bis-(μ -oxo) dimer, was seen in these experiments. Filtration of the present solution removed trace brown solids (probably MnO_2 from trace Mn impurities), after which excess NH_4PF_6 was then added to the solution to initiate the precipitation of PF_6^- salts.

The product isolated at this point depends on slight adjustments in reaction conditions (**Figure 71b**). When this reaction occurs at low ($< 0.01\text{M}$) concentrations, precipitation occurs slowly over the course of several days to yield thin orange plates of a $[\text{Mn}(\text{B14N4})(\text{OH})(\text{OAc})]^+$ mixed salt. This compound is only the third example of a structurally characterized mononuclear manganese(III) hydroxide complex.¹⁸⁴ Such species have recently been implicated as intermediates in O_2 production from the oxygen evolving complex of photosynthesis.¹⁸⁵ Intriguingly, the acetate ligand, which helps stabilize the hydroxo complex through an intramolecular hydrogen bond (*vide infra*), must be produced *in situ* by oxidation of the ethanol cosolvent, almost certainly by some $\text{Mn}(\text{B14N4})^{n+}$ oxidant. No other source of acetate ions is available, because only chloride and PF_6^- salts have been introduced to the system. Other studies have shown $\text{Mn}(\text{B14N4})\text{Cl}_2$ to be a relatively poor catalyst for the oxidation of alcohols, but it does have some small turnover,¹⁸⁶ as further indicated by the fact that the $\text{Mn}(\text{B14N4})(\text{OH})(\text{OAc})^+$ cation and a coprecipitate of another acetate salt are formed. A slow catalytic reaction would also explain the very slow, steady precipitation of the product over the course of several days.

If the above reaction is carried out at high concentrations (> 0.6 M), an immediate precipitate of a sticky orange powder is formed upon addition of the ammonium hexafluorophosphate. Ether diffusion into a methanol solution of this crude product gives dark red crystals of $[\text{Mn}(\text{B14N4})(\text{OMe})_2]\text{PF}_6$, along with a pale orange coprecipitate. Again, since no methanol or methoxy anion is present in the reaction, it is likely that the ill-characterized crude product attacks the methanol recrystallizing solvent to give the dimethoxy product. From the chloride replacement reactions, titration data, and the structure of the monohydroxo complex, it seems logical to suggest a dihydroxo Mn^{3+} species as the likely intermediate along the way to formation of the dimethoxy complex. The same species is probably present in the reaction conducted at low concentrations, giving the monohydroxo product as well, but at higher concentrations the PF_6^- salt precipitates before the oxidation of ethanol to acetate can occur. Efforts are continuing to isolate this putative dihydroxo complex for further characterization, but have thus far been thwarted by the impurity of crude products and their reactivity with recrystallizing solvents.

Representations of the crystal structures of $[\text{Mn}(\text{B14N4})(\text{N}_3)_2]\text{PF}_6$, $[\text{Mn}(\text{B14N4})(\text{OH})(\text{OAc})]\text{PF}_6$, and $[\text{Mn}(\text{B14N4})(\text{OMe})_2]\text{PF}_6$ are found in **Figure 72**. The $\text{N}_{\text{eq}}\text{-Mn-}\text{N}_{\text{eq}}$ and $\text{N}_{\text{ax}}\text{-Mn-}\text{N}_{\text{ax}}$ bond angles are not significantly different from those of $\text{Mn}(\text{B14N4})\text{Cl}_2^+$ (*vide supra*). $\text{Mn}(\text{B14N4})(\text{N}_3)_2^+$: axial bond angle $\text{N}(4)\text{-Mn}(1)\text{-N}(4\text{A}) = 173.4(2)^\circ$, equatorial bond angle $\text{N}(1)\text{-Mn}(1)\text{-N}(1\text{A}) = 83.1(2)^\circ$. $\text{Mn}(\text{B14N4})(\text{OH})(\text{OAc})^+$: equatorial bond angle $\text{N}(1)\text{-Mn}(1)\text{-N}(8) = 168.9(2)^\circ$, equatorial bond angle $\text{N}(4)\text{-Mn}(1)\text{-N}(11) = 83.4(2)^\circ$. $\text{Mn}(\text{B14N4})(\text{OMe})_2^+$: axial bond

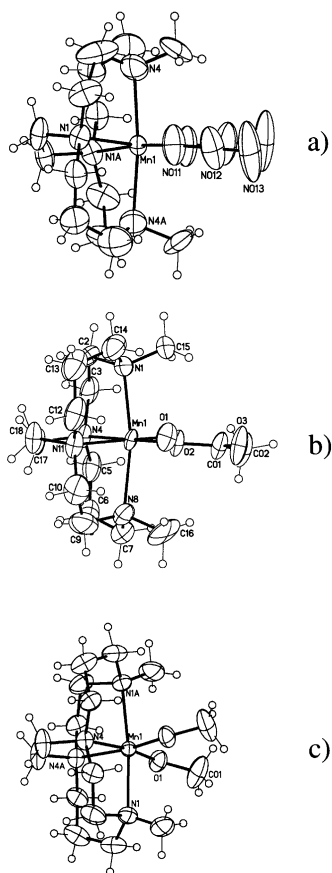


Figure 72. Molecular structures of
 a) $\text{Mn}(\text{Me}_2\text{B14N4})(\text{N}_3)_2^+$,
 b) $\text{Mn}(\text{Me}_2\text{B14N4})(\text{OH})(\text{OAc})^+$, and
 c) $\text{Mn}(\text{Me}_2\text{B14N4})(\text{OMe})_2^+$

angle $\text{N}(1)\text{-Mn}(1)\text{-N}(1\text{A}) = 166.31(9)^\circ$, equatorial bond angle $\text{N}(4)\text{-Mn}(1)\text{-N}(4\text{A}) = 81.76(8)^\circ$. This indicates that the Mn^{3+} ion has a relatively rigidly defined cavity to occupy within ligand B14N4. Other selected bond lengths and angles can be found in **Table 16**. The bis-azido complex has almost linear azide ligands, with $\text{N}(011)\text{-N}(012)\text{-N}(013) = 177.7(7)^\circ$.

The most interesting of these structures is the hydroxo complex $\text{Mn}(\text{B14N4})(\text{OH})(\text{OAc})^+$. As stated above, this is only the third structurally characterized monomeric manganese(III) hydroxo complex.¹⁸⁴ The pertinent metrical parameters are $\text{Mn}(1)\text{-O}(1) = 1.812(4) \text{ \AA}$, $\text{Mn}(1)\text{-O}(2) = 1.965(4) \text{ \AA}$, and the interatomic distance between O(1) and O(3) is

2.766 \AA . The Mn-hydroxo bond length is consistent with the other two mononuclear manganese(III)-OH structures,¹⁸⁴ which have distances of $1.816(4) \text{ \AA}$ and $1.827(3) \text{ \AA}$, respectively, but is slightly shorter than either of these and much longer than the Mn-O(acetate) bond. A possible explanation for the slightly shorter bond length in the present case is that the ligand B14N4 is neutral which might dissipate some of the Mn-O attraction, while the polydentate ligands in both previous structures bear multiple negative charges. Interestingly, an intramolecular hydrogen bonding

Table 16. Selected bond lengths (Å) and angles (°) for $\text{Mn}(\text{Me}_2\text{B14N4})(\text{N}_3)_2^+$, $\text{Mn}(\text{Me}_2\text{B14N4})(\text{OH})(\text{OAc})^+$, and $\text{Mn}(\text{Me}_2\text{B14N4})(\text{OMe})_2^+$

(i) For $\text{Mn}(\text{Me}_2\text{B14N4})(\text{N}_3)_2^+$			
Mn(1)-N(011)	1.929(4)	Mn(1)-N(4)	2.306(5)
Mn(1)-N(1)	2.099(3)		
N(011)#1-Mn(1)-N(011)	97.7(3)	N(1)-Mn(1)-N(4)	81.7(2)
N(011)-Mn(1)-N(1)#1	170.5(2)	N(011)-Mn(1)-N(4)#1	92.3(2)
N(011)-Mn(1)-N(1)	89.9(2)	N(1)-Mn(1)-N(4)#1	93.3(2)
N(011)-Mn(1)-N(4)	92.1(2)	N(4)-Mn(1)-N(4)#1	173.4(2)
(ii) For $\text{Mn}(\text{Me}_2\text{B14N4})(\text{OH})(\text{OAc})^+$			
Mn(1)-O(1)	1.812(4)	Mn(1)-N(11)	2.157(5)
Mn(1)-O(2)	1.965(4)	Mn(1)-N(1)	2.248(5)
Mn(1)-N(4)	2.110(5)	Mn(1)-N(8)	2.298(6)
O(1)-Mn(1)-O(2)	96.6(2)	N(4)-Mn(1)-N(1)	83.2(2)
O(1)-Mn(1)-N(4)	172.1(2)	N(11)-Mn(1)-N(1)	89.6(2)
O(2)-Mn(1)-N(4)	89.4(2)	O(1)-Mn(1)-N(8)	96.5(2)
O(1)-Mn(1)-N(11)	91.3(2)	O(2)-Mn(1)-N(8)	90.4(2)
O(2)-Mn(1)-N(11)	169.5(2)	N(4)-Mn(1)-N(8)	88.6(2)
N(4)-Mn(1)-N(11)	83.4(2)	N(11)-Mn(1)-N(8)	81.9(2)
O(1)-Mn(1)-N(1)	90.9(2)	N(1)-Mn(1)-N(8)	168.9(2)
O(2)-Mn(1)-N(1)	97.0(2)		
(iii) For $\text{Mn}(\text{Me}_2\text{B14N4})(\text{OMe})_2^+$			
Mn(1)-O(1)	1.838(2)	Mn(1)-N(1)	2.344(2)
Mn(1)-N(4)	2.137(2)		
O(1)#1-Mn(1)-O(1)	102.83(10)	O(1)-Mn(1)-N(1)	96.25(7)
O(1)#1-Mn(1)-N(4)	87.78(7)	N(4)-Mn(1)-N(1)	80.45(7)
O(1)-Mn(1)-N(4)	169.05(7)	N(4)#1-Mn(1)-N(1)	89.18(7)
N(4)-Mn(1)-N(4)#1	81.76(8)	N(1)-Mn(1)-N(1)#1	166.31(9)
O(1)#1-Mn(1)-N(1)	92.28(7)		

hydrogen bonds, although they are intermolecular, between pairs of $\text{Mn}^{\text{III}}(\text{OH})$ molecules in this case.^{184b}

The electronic properties of these additional $\text{Mn}(\text{B14N4})^{3+}$ complexes have been briefly probed using electronic spectroscopy and cyclic voltammetry. The electronic spectra of $[\text{Mn}(\text{B14N4})(\text{N}_3)_2]^+$, $[\text{Mn}(\text{B14N4})(\text{OH})(\text{OAc})]^+$, and $[\text{Mn}(\text{B14N4})(\text{OMe})_2]^+$ in acetonitrile¹⁶⁷ are shown in **Figure 73** and summarized in **Table 17**. The azide complex has an electronic spectrum very similar in appearance to the dichloride complex (*vide supra*), except that the wavelength and the extinction coefficient of the lowest energy charge transfer band is much different, which is not unusual for charge transfer bands when changing the nature of the ligand (azide for

interaction stabilizes the hydroxo ligand in this structure. The carbonyl oxygen of the bound acetato ligand is only 2.766 Å away from the hydroxo oxygen, suggesting a hydrogen bond between them, although the hydrogen atom was not found in the structure solution. One other $\text{Mn}^{\text{III}}(\text{OH})$ species is also stabilized by

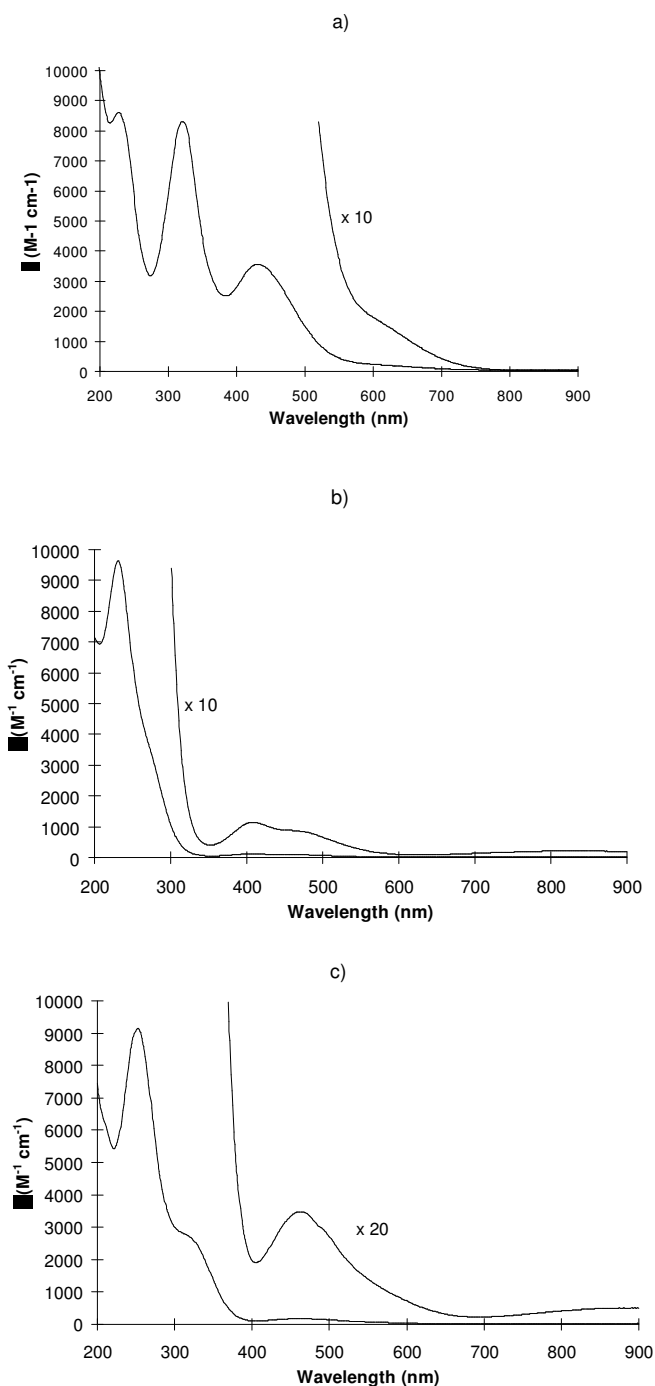


Figure 73. Electronic spectra of $\text{Mn}(\text{Me}_2\text{B14N4})(\text{N}_3)_2^+$, b) $\text{Mn}(\text{Me}_2\text{B14N4})(\text{OH})(\text{OAc})^+$, and c) $\text{Mn}(\text{Me}_2\text{B14N4})(\text{OMe})_2^+$

chloride). The other two charge transfer bands are somewhat altered in the azide complex, but not as drastically. Also in the azide complex, a low energy shoulder appears at ~ 625 nm which may correspond to an allowed d-d absorption (*vide supra*). The spectra of the hydroxo and dimethoxy complexes are distinctly different from the dichloride complex, while strongly resembling each another. Only one very strong charge transfer band (although the dimethoxy complex has a weak shoulder as well) is seen at high energy for these two complexes, while the dichloride and bis-azido complexes exhibit two such bands. In addition, these complexes with oxygen ligands have a somewhat resolved band at lower energy

Table 17. Electronic spectra of $\text{Mn}(\text{Me}_2\text{B14N4})^{3+}$ complexes in MeCN

Complex	Absorption Bands [nm] (Extinction Coefficient) [$\text{M}^{-1} \text{cm}^{-1}$]
$[\text{Mn}(\text{Me}_2\text{B14N4})(\text{N}_3)_2]\text{PF}_6$	227(8600), 321(8310), 433(3570), 625(170)
$[\text{Mn}(\text{Me}_2\text{B14N4})(\text{OH})(\text{OAc})]\text{PF}_6$	231(9640), 409(110), 478sh(80)
$[\text{Mn}(\text{Me}_2\text{B14N4})(\text{OMe})_2]\text{PF}_6$	252(9140), 324sh(2600), 464(170)

whose extinction coefficients are consistent with d-d bands, but whose energies appear too high for that assignment.¹⁶⁵

The cyclic voltammograms (**Figure 74**, **Table 18**) of the $\text{Mn}(\text{B14N4})^{3+}$ complexes show much greater differences in behavior. The azide complex¹⁶⁷ has

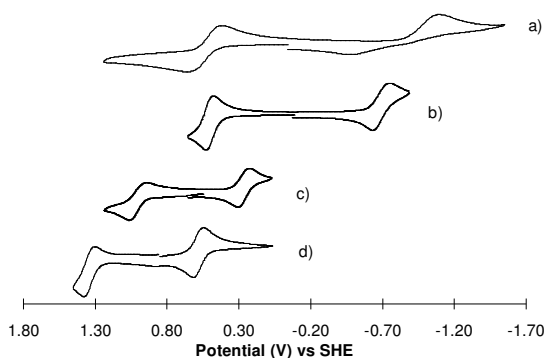


Figure 74. Cyclic voltammograms of a) $\text{Mn}(\text{Me}_2\text{B14N4})(\text{OMe})_2^+$, b) $\text{Mn}(\text{Me}_2\text{B14N4})(\text{OH})(\text{OAc})^+$, c) $\text{Mn}(\text{Me}_2\text{B14N4})(\text{N}_3)_2^+$, and d) $\text{Mn}(\text{Me}_2\text{B14N4})\text{Cl}_2^+$

$\text{Mn}^{3+}/\text{Mn}^{2+}$ and $\text{Mn}^{4+}/\text{Mn}^{3+}$ couples similar in reversibility to those of the chloride complex, but the $E_{1/2}$ potentials of these waves are about 300 mV less positive (**Figure 74c-d**). The hydroxo-acetato complex is even more drastically effected in its redox potentials. In this complex, the $\text{Mn}^{3+}/\text{Mn}^{2+}$ wave has been displaced to a quite negative potential, -0.689 V, and the $\text{Mn}^{4+}/\text{Mn}^{3+}$ wave is now only +0.505 V positive from SHE

(**Figure 74b**). This is an easily achievable potential with common oxidants, and along with the aqueous titration data, helps explain why the parent complex is a useful aqueous oxidation catalyst.²³ The titration data says that at least one hydroxo group is bound at most relevant pH's ($\text{pK}_{a1} = 1.6(2)$) and two hydroxo groups are

Table 18. Electrochemistry of M³⁺ complexes in MeCN

Complex	Redox Couple	E _{1/2} (V)	(E _a -E _c) (mv)
[Fe(Me ₂ B12N4)Cl ₂] ₂ PF ₆	Fe ³⁺ /Fe ²⁺	+0.026	60
[Fe(Me ₂ B14N4)Cl ₂] ₂ PF ₆	Fe ³⁺ /Fe ²⁺	+0.106	79
[Mn(Me ₂ B12N4)Cl ₂] ₂ PF ₆	Mn ³⁺ /Mn ²⁺	+0.400	71
	Mn ⁴⁺ /Mn ³⁺	+1.177	76
[Mn(Me ₂ B14N4)Cl ₂] ₂ PF ₆	Mn ³⁺ /Mn ²⁺	+0.582	72
	Mn ⁴⁺ /Mn ³⁺	+1.343	76
[Mn(Me ₂ B14N4)(N ₃)] ₂ PF ₆	Mn ³⁺ /Mn ²⁺	+0.269	81
	Mn ⁴⁺ /Mn ³⁺	+1.005	118
[Mn(Me ₂ B14N4)(OH)(OAc)] ₂ PF ₆	Mn ³⁺ /Mn ²⁺	-0.689	132
	Mn ⁴⁺ /Mn ³⁺	+0.505	62
[Mn(Me ₂ B14N4)(OMe) ₂] ₂ PF ₆	Mn ³⁺ /Mn ²⁺	-0.781	628
	Mn ⁴⁺ /Mn ³⁺	+0.542	243

bound under basic conditions (pK_{a2} = 5.87(2)). If the dihydroxo complex has similar oxidation potentials to the hydroxo-acetato analogue, then oxidation to higher metal oxidation states should be relatively easy, facilitating any high valent metal-centered substrate

oxidations. A similar effect is found for the dimethoxy complex (**Figure 74a**). Though much less reversible, probably due to the dissociation of methoxide upon reduction, the Mn³⁺/Mn²⁺ potential is even more negative than in the hydroxo complex, at -0.781 V. The Mn⁴⁺/Mn³⁺ potential is just slightly more positive than in the hydroxo case, at +0.542 V.

In summary, Fe²⁺ and Mn²⁺, as noted in the introduction, are enormously important biological ions. However, their properties have made them difficult to control in oxygenated aqueous systems without the protection of the bulky, hydrophobic proteins provided by nature. The ligands B14N4 and B12N4 are ideally suited to do just that--keep Mnⁿ⁺ and Feⁿ⁺ stable in aqueous solutions and under other harsh conditions to take advantage of their known catalytic reactivity. Here, is reported the synthesis of Mn²⁺ and Fe²⁺ complexes of these cross-bridged

macrobicyclic ligands, overcoming their proton-sponge nature by reducing the activity of protons in the reaction mixture. Also reported are the synthesis of Mn^{3+} and Fe^{3+} complexes by the facile chemical oxidation of their divalent metal ion analogues, utilizing Br_2 as oxidant. Using these simple, but topologically constrained ligands, complexes which are all high spin yet remarkably stable in various solvents have been produced. The extent to which counter ions (Cl^-) are dissociated increases with the dielectric constant of the solvent resulting in their complete replacement by solvent in water, which produces the two labile *cis* sites needed for many types of catalysis.¹³⁹ Potentiometric titrations of $\text{Mn}(\text{B14N4})\text{Cl}_2$ and $\text{Mn}(\text{B14N4})\text{Cl}_2^+$ reveal the facile deprotonation of the water molecules that replace chloro ligands upon dissolution. The manganese complexes exhibit readily detectable higher oxidation states of +3 and +4, whereas the iron complexes show only the divalent and trivalent states. Such stabilization of multiple oxidation states is again necessary for various catalytic cycles. The coordination spheres of the metal complexes are comparable, but the smaller ring is more distorted in its pseudo octahedral complexes because these metal ions are a bit larger than would be ideal for occupancy. The derivatives of the larger rings are harder to oxidize, which can be traced to a better size match between the larger ring and the larger di- or trivalent ions and the smaller rings with the smaller tri- or tetravalent ions. Several additional derivatives of the Mn^{3+} -B14N4 combination have been prepared. Simple ligand replacement reactions have given the bis-azido complex, which has similar properties to the dichloro parent complex. Alternative oxidation reactions of the divalent precursor complex by air in aqueous solution has yielded both a mono-hydroxo complex, stabilized by an intramolecular hydrogen bond from an acetate group created by the *in situ* oxidation of ethanol cosolvent, and a dimethoxy complex, possibly the decomposition product in methanol of a reactive dihydroxo complex. Importantly, no evidence of oxo- or hydroxo-bridged dimers or polymers has been seen under conditions normally associated with

their formation,^{182,183} probably due to steric interactions of the ligand methyl groups. These dimethoxy and hydroxo complexes have greatly lowered Mn⁴⁺/Mn³⁺ redox couples that may be the key to the usefulness of these species as aqueous oxidation catalysts.²³

Complexes of Unsubstituted and Benzyl Substituted Ligands

Above is described the synthesis and characterization of Fe²⁺ and Mn²⁺ complexes of the methyl-substituted ligands B14N4 and B12N4, and their one-electron oxidized analogues. These compounds have exciting properties such as remarkable stabilities in harsh aqueous conditions and easily accessible higher oxidation states that suggest useful applications as aqueous oxidation catalysts. Below, the synthesis, X-ray crystal structures and electrochemical behavior of similar complexes where the ligands have been slightly altered to probe the effect on the metal center. Ligands having benzyl groups or simple hydrogens (“unsubstituted ligands”) as the two nitrogen substituents¹¹³ were complexed to the metal ions of interest. The characterization of these new complexes and comparison of them to the methyl-substituted “parent” ligand complexes is presented.

Complex Synthesis. The Fe²⁺ and Mn²⁺ complexes with “parent” ligands B14N4 and B12N4 were prepared from the corresponding anhydrous M(py)₂Cl₂ starting material in CH₃CN. Unfortunately, complexation of Bn₂B14N4 and Bn₂B12N4 via the same reaction was not successful. There are several possible explanations, including decreased solubility of the ligands in acetonitrile, increased steric bulk (the benzyl groups) near the ligand cavity, and/or increased ligand basicity, although the latter has not been confirmed. Several sets of reaction conditions were investigated until success was achieved in 1:1 triethylamine:acetonitrile solution, both from triflate and dichlorobis-pyridine metal starting materials. Triethylamine is generally used as a mild base in complexation reactions, but was found to be a good

solvent for the ligands, which are not readily soluble in many of the aprotic solvents deemed necessary for complexation of these ligands. Complexation of the unsubstituted ligands H₂B14N4 and H₂B12N4 proved less challenging, and followed protocols established with the “parent” ligands, except for the substitution of DMF as the solvent.

Finally, the air oxidation of the complexes with H₂B14N4 and H₂B12N4 have been studied. One possible result is ligand oxidation, as secondary amines are notoriously easy to oxidize to imines in their transition metal complexes.¹⁸⁷ Another possible reaction is metal ion oxidation and formation of oxo- or hydroxo-bridged dimers. Experimentally, the Fe²⁺ complexes of both of these ligands immediately turn from pale yellow to deep red-brown in solution when exposed to air. This behavior does not occur in the Fe²⁺ complexes with ligands Bn₂B14N4, Bn₂B12N4, B14N4, or B14N4; their solutions only become somewhat darker yellow in color under the same conditions. Cache[®] molecular modeling studies informed us that dimerization of the latter complexes should be sterically inhibited by the N-alkyl groups, which would need to occupy the same space as the second ligand in a typical μ-oxo dimer. These same modeling studies revealed that no such steric problems existed for the unsubstituted ligands H₂B14N4 and H₂B12N4. As expected, monomers of these ligand complexes do indeed form μ-oxo Fe³⁺ dimers familiar to coordination chemistry¹⁸² upon oxidation by air, but no ligand oxidation is observed. The products of these reactions have been structurally characterized (*vide infra*).

The manganese(II) complexes with the methyl-substituted ligand B14N4 has been extensively studied under conditions favorable for dimerization, and no such reaction has yet been observed. In contrast, the Mn²⁺ complex of H₂B12N4 immediately turns from colorless to deep green upon exposure of a DMF solution to air. The solution has the characteristic 16-line EPR signal (**Figure 75**), in addition to its telling color, associated with a Mn³⁺/Mn⁴⁺ oxo-bridged dimer.¹⁸³ Surprisingly the

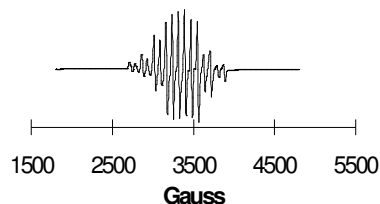


Figure 75. 77 K EPR spectrum of air oxidized $\text{Mn}(\text{H}_2\text{B12N4})\text{Cl}_2$

manganese(II) complex of $\text{H}_2\text{B14N4}$ turns a pale red color under the same conditions and does not have the 16-line EPR. Obviously, a different reaction, for reasons possibly other than steric ones, since the iron complex of this ligand can dimerize, occurs upon air oxidation of this compound. Neither of the products from the air oxidation of these Mn^{2+} precursors has been

satisfactorily characterized.

Crystal Structures. X-ray crystal structures for two of the three monomeric

complexes with dibenzyl ligands, are shown in **Figure 76**. Metrical parameters are collected in **Table 19**.

These structures confirm the expected geometric properties of the cross-bridged ligands, which are constrained by the short cross-bridge to folded conformations. As in the parent ligand complexes, the macrobicycle occupies two axial and two *cis* equatorial sites of distorted octahedra, while the remaining *cis* equatorial sites are occupied by either two triflate ligands or two chloride ligands.

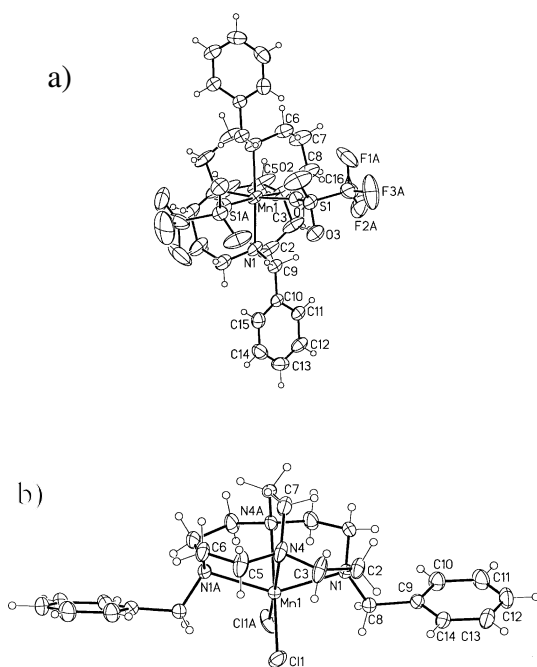


Figure 76. Molecular structures of a) $\text{Mn}(\text{Bn}_2\text{B14N4})(\text{CF}_3\text{SO}_3)_2$ and b) $\text{Mn}(\text{Bn}_2\text{B12N4})\text{Cl}_2$

Inspection of the three structures reveals several continuing

Table 19. Selected bond lengths (Å) and angles (deg) for benzyl-substituted cross-bridged ligand complexes

(i) For Mn(Bn₂B14N4)(CF₃SO₃)₂			
Mn(1)-O(1)#1	2.153(2)	S(1)-O(3)	1.428(2)
Mn(1)-N(4)	2.266(2)	S(1)-O(1)	1.452(2)
Mn(1)-N(1)	2.295(2)	S(1)-C16Aa	1.852(12)
S(1)-O(2)	1.424(2)		
O(1)#1-Mn(1)-O(1)	94.93(9)	N(4)-Mn(1)-N(1)#1	87.58(8)
O(1)-Mn(1)-N(4)	93.11(9)	O(1)-Mn(1)-N(1)	97.26(7)
O(1)-Mn(1)-N(4)#1	170.40(9)	N(4)-Mn(1)-N(1)	81.06(9)
N(4)-Mn(1)-N(4)#1	79.40(14)	N(1)#1-Mn(1)-N(1)	165.25(10)
O(1)-Mn(1)-N(1)#1	92.71(7)		
(ii) For Mn(Bn₂B12N4)Cl₂			
Mn(1)-N(4)	2.3051(13)	Mn(1)-Cl(1)	2.4276(4)
Mn(1)-N(1)	2.3311(12)		
N(4)-Mn(1)-N(4)#1	74.56(8)	N(4)#1-Mn(1)-Cl(1)	168.60(4)
N(4)-Mn(1)-N(1)#1	77.69(4)	N(1)#1-Mn(1)-Cl(1)	102.55(3)
N(4)#1-Mn(1)-N(1)#1	74.06(4)	N(1)-Mn(1)-Cl(1)	100.84(3)
N(1)#1-Mn(1)-N(1)	144.30(6)	Cl(1)-Mn(1)-Cl(1)#1	97.21(3)
N(4)-Mn(1)-Cl(1)	94.13(4)		
(iii) For Fe(Bn₂B12N4)Cl₂			
Fe(1)-N(4)	2.234(2)	Fe(1)-Cl(1)	2.4004(5)
Fe(1)-N(1)	2.2757(14)		
N(4)#1-Fe(1)-N(4)	76.92(9)	N(1)-Fe(1)-Cl(1)	99.18(4)
N(4)-Fe(1)-N(1)#1	79.21(5)	N(4)-Fe(1)-Cl(1)#1	171.26(5)
N(4)-Fe(1)-N(1)	75.63(6)	N(1)-Fe(1)-Cl(1)#1	102.61(4)
N(1)#1-Fe(1)-N(1)	147.71(8)	Cl(1)-Fe(1)-Cl(1)#1	94.39(3)
N(4)-Fe(1)-Cl(1)	94.35(5)		

74.56(8)° for Mn(Bn₂B14N4)(CF₃SO₃)₂ and Mn(Bn₂B12N4)Cl₂, respectively. The smaller angles for the smaller macrobicyclic demonstrate how the metal ion is less engulfed in the ligand cavity. Surprisingly, the triflate complex of Bn₂B14N4 contains a Mn²⁺ ion deeper in the ligand cleft than in the related dichloro complex of B14N4. This previously discussed structure has the N_{ax}-M-N_{ax} bond angle for Mn(B14N4)Cl₂ at 158.0(2)° and the N_{eq}-M-N_{eq} angle is 75.6(2)°. These angles are several degrees smaller than in Mn(Bn₂B14N4)(CF₃SO₃)₂ (see above). It might be expected that the more bulky triflate ligands in the complex of Bn₂B14N4 would act to draw the Mn²⁺ ion further out of the ligand cleft than monatomic chlorides of the complex of B14N4. Instead the opposite is observed as the larger N-M-N angles for Mn(Bn₂B14N4)(CF₃SO₃)₂ indicate. It appears that there is sufficient space around the

trends. First, the size of the ring system dictates the distortion of the octahedra. The 14-membered ring in Bn₂B14N4, engulfs the metal ion more fully than does the 12-membered ring in Bn₂B12N4. The N_{ax}-M-N_{ax} bond angle for Mn(Bn₂B14N4)(CF₃SO₃)₂ is 165.25(10)°, while for Mn(Bn₂B12N4)Cl₂, it is only 144.30(6)°. Likewise, the N_{eq}-M-N_{eq} angles are 79.40(14)° and

equator of this complex, since the benzyl groups are extended axially, to accommodate the two triflate ligands without costly steric interactions. As such, it is logical that the smaller triflate oxygens bound to Mn^{2+} would allow this ion deeper access to the ligand cavity than the larger chloro ligands of $\text{Mn}(\text{B14N4})\text{Cl}_2$, which would require more space. Electronic factors might also contribute; the poorly complementary triflate ligands don't add enough electron density, so the metal ion has to delve deeper into the tetradentate ligand cavity. The phenomenon is also born out in the larger Cl-Mn-Cl angle ($98.85(6)^\circ$) in $\text{Mn}(\text{B14N4})\text{Cl}_2$, versus that of the O-Mn-O angle ($94.93(9)^\circ$) in $\text{Mn}(\text{Bn}_2\text{B14N4})(\text{CF}_3\text{SO}_3)_2$, the larger chloride atoms requiring more spatial separation.

The second observation is that the smaller Fe^{2+} ion is more fully engulfed by macrobicycle $\text{Bn}_2\text{B12N4}$ than is the larger Mn^{2+} ion, as seen before in the parent ligand complexes. $\text{N}_{\text{ax}}\text{-M-N}_{\text{ax}}$ is $147.71(8)^\circ$ for $\text{Fe}(\text{Bn}_2\text{B12N4})\text{Cl}_2$ while this angle is $144.30(6)^\circ$ for $\text{Mn}(\text{Bn}_2\text{B12N4})\text{Cl}_2$. The $\text{N}_{\text{eq}}\text{-M-N}_{\text{eq}}$ angles are $76.92(9)^\circ$ and $74.56(8)^\circ$ for $\text{Fe}(\text{Bn}_2\text{B12N4})\text{Cl}_2$ and $\text{Mn}(\text{Bn}_2\text{B12N4})\text{Cl}_2$, respectively. In these two complexes, the average Fe-N distance is 2.255 \AA , while the average Mn-N distance is 2.318 \AA , confirming the size relationship of the Fe^{2+} and Mn^{2+} cations. These relationships, macrocycle ring size and metal ionic radius influencing how deep the metal ion resides within the ligand cavity, determine how close to truly octahedral the coordination geometry is, and they have been consistently observed with several different metal ions and ligand ring sizes.

Finally, the intermolecular interactions of the two ligand $\text{Bn}_2\text{B12N4}$ complexes in the solid state should be noted. The benzyl groups extending from the macrobicyclic complexes have classical $\pi\text{-}\pi$ interactions with benzyl groups from neighboring molecules, as demonstrated in the crystal packing diagram of $\text{Fe}(\text{Bn}_2\text{B12N4})\text{Cl}_2$, shown in **Figure 77**. These interactions have the two benzyl groups in the appropriately “slipped” arrangement where one aromatic carbon is

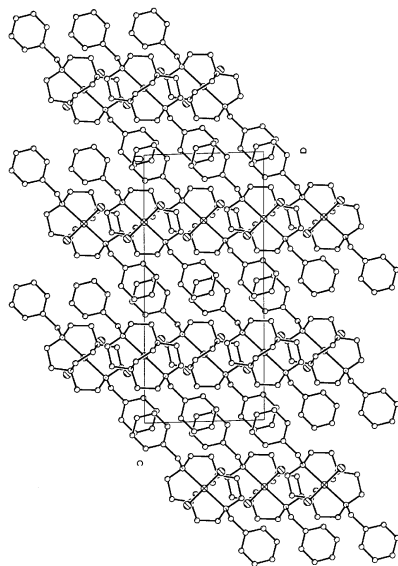


Figure 77. Crystal packing diagram for $\text{Fe}(\text{Bn}_2\text{B12N4})\text{Cl}_2$

directly above the centroid of its partner's aromatic ring.¹⁸⁸ The paired benzyl groups are found 3.32 Å apart, also an accepted distance for this type of interaction.¹⁸⁸ These interactions may contribute to the general low solubilities of the complexes of $\text{Bn}_2\text{B14N4}$ and $\text{Bn}_2\text{B12N4}$, because of the strengths of these interactions in the solid state.

The crystal structures of dimeric iron(III) complexes of

$\text{H}_2\text{B14N4}$ and $\text{H}_2\text{B12N4}$ are represented in **Figure 78**. Metrical parameters can be found in **Table 20**. The Fe^{3+} ions of these complexes are again found in pseudo

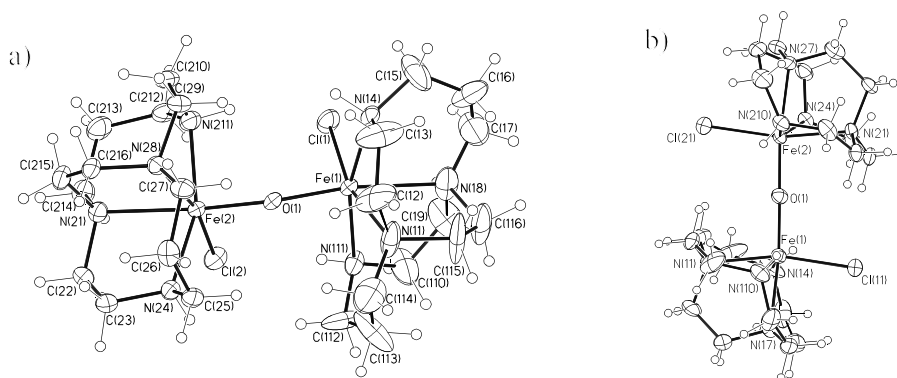


Figure 78. Molecular structures of a) $[\text{Cl}(\text{H}_2\text{B14N4})\text{Fe}(\mu\text{-O})\text{Fe}(\text{H}_2\text{B14N4})\text{Cl}]^{2+}$ and b) $[\text{Cl}(\text{H}_2\text{B12N4})\text{Fe}(\mu\text{-O})\text{Fe}(\text{H}_2\text{B12N4})\text{Cl}]^{2+}$

octahedral six coordinate geometries, similar to most monomeric complexes of the methyl- and benzyl substituted ligands. Commonly, such dimers have a coordination

Table 20. Selected bond lengths (Å) and angles (°) for unsubstituted cross-bridged ligand complexes

(i) For $[\text{Cl}(\text{H}_2\text{B14N4})\text{Fe}(\mu\text{-O})\text{Fe}(\text{H}_2\text{B14N4})\text{Cl}]^{2+}$			
Fe(1)-O(1)	1.831(4)	O(1)-Fe(2)	1.820(4)
Fe(1)-N(111)	2.145(5)	Fe(2)-N(211)	2.157(5)
Fe(1)-N(14)	2.157(5)	Fe(2)-N(24)	2.152(5)
Fe(1)-N(11)	2.180(5)	Fe(2)-N(28)	2.207(5)
Fe(1)-N(18)	2.283(6)	Fe(2)-N(21)	2.287(5)
Fe(1)-Cl(1)	2.368(2)	Fe(2)-Cl(2)	2.350(2)
O(1)-Fe(1)-N(111)	95.2(2)	O(1)-Fe(2)-N(211)	94.9(2)
O(1)-Fe(1)-N(14)	98.6(2)	O(1)-Fe(2)-N(24)	101.5(2)
N(111)-Fe(1)-N(14)	163.6(2)	N(211)-Fe(2)-N(24)	159.6(2)
O(1)-Fe(1)-N(11)	95.4(2)	O(1)-Fe(2)-N(28)	94.9(2)
N(111)-Fe(1)-N(11)	88.3(2)	N(211)-Fe(2)-N(28)	81.6(2)
N(14)-Fe(1)-N(11)	81.8(2)	N(24)-Fe(2)-N(28)	85.1(2)
O(1)-Fe(1)-N(18)	171.8(2)	O(1)-Fe(2)-N(21)	173.9(2)
N(111)-Fe(1)-N(18)	79.3(2)	N(211)-Fe(2)-N(21)	82.7(2)
N(14)-Fe(1)-N(18)	85.9(2)	N(24)-Fe(2)-N(21)	79.7(2)
N(11)-Fe(1)-N(18)	78.5(2)	N(28)-Fe(2)-N(21)	79.2(2)
O(1)-Fe(1)-Cl(1)	98.50(12)	O(1)-Fe(2)-Cl(2)	98.42(13)
N(111)-Fe(1)-Cl(1)	93.96(14)	N(211)-Fe(2)-Cl(2)	97.56(14)
N(14)-Fe(1)-Cl(1)	92.6(2)	N(24)-Fe(2)-Cl(2)	91.83(13)
N(11)-Fe(1)-Cl(1)	165.7(2)	N(28)-Fe(2)-Cl(2)	166.63(13)
N(18)-Fe(1)-Cl(1)	88.03(14)	N(21)-Fe(2)-Cl(2)	87.42(13)
Fe(2)-O(1)-Fe(1)	144.1(2)		
(ii) For $[\text{Cl}(\text{H}_2\text{B12N4})\text{Fe}(\mu\text{-O})\text{Fe}(\text{H}_2\text{B12N4})\text{Cl}]^{2+}$			
Fe(1)-O(1)	1.818(4)	Fe(2)-O(1)	1.807(4)
Fe(1)-N(14)	2.149(6)	Fe(2)-N(210)	2.174(5)
Fe(1)-N(110)	2.160(5)	Fe(2)-N(24)	2.188(5)
Fe(1)-N(11)	2.173(5)	Fe(2)-N(21)	2.198(5)
Fe(1)-N(17)	2.257(5)	Fe(2)-N(27)	2.266(5)
Fe(1)-Cl(11)	2.349(2)	Fe(2)-Cl(21)	2.354(2)
O(1)-Fe(1)-N(14)	101.2(2)	O(1)-Fe(2)-N(24)	103.2(2)
O(1)-Fe(1)-N(110)	103.1(2)	N(210)-Fe(2)-N(24)	146.8(2)
N(14)-Fe(1)-N(110)	148.3(2)	O(1)-Fe(2)-N(21)	94.9(2)
O(1)-Fe(1)-N(11)	96.3(2)	N(210)-Fe(2)-N(21)	79.9(2)
N(14)-Fe(1)-N(11)	78.7(2)	N(24)-Fe(2)-N(21)	76.1(2)
N(110)-Fe(1)-N(11)	78.7(2)	O(1)-Fe(2)-N(27)	172.1(2)
O(1)-Fe(1)-N(17)	174.0(2)	N(210)-Fe(2)-N(27)	74.6(2)
N(14)-Fe(1)-N(17)	77.2(2)	N(24)-Fe(2)-N(27)	78.1(2)
N(110)-Fe(1)-N(17)	76.4(2)	N(21)-Fe(2)-N(27)	77.7(2)
N(11)-Fe(1)-N(17)	77.7(2)	O(1)-Fe(2)-Cl(21)	97.82(14)
O(1)-Fe(1)-Cl(11)	98.02(14)	N(210)-Fe(2)-Cl(21)	98.6(2)
N(14)-Fe(1)-Cl(11)	99.1(2)	N(24)-Fe(2)-Cl(21)	99.83(14)
N(110)-Fe(1)-Cl(11)	97.3(2)	N(21)-Fe(2)-Cl(21)	167.23(14)
N(11)-Fe(1)-Cl(11)	165.6(2)	N(27)-Fe(2)-Cl(21)	89.62(14)
N(17)-Fe(1)-Cl(11)	87.95(14)	Fe(2)-O(1)-Fe(1)	178.9(3)
O(1)-Fe(2)-N(210)	101.4(2)		

number of 5, although 6- and 7- coordinate dimers are known.¹⁸² It is interesting that the monodentate chloro ligands are maintained in the present structures, but since the macrobicyclic ligands are uncharged, the only Coulombic forces influencing the monoanionic halide are attractive. Also, the folded ligand conformations help separate the ligands from each other, easing the steric interactions that might favor lower coordination numbers with more planar ligands. As mentioned earlier, there appears to be no ligand oxidation during the exposure to the moist oxidation process that led to these dimers--all of the

C-N bond lengths are within the accepted values for single bonds.¹⁸⁹ Such ligand oxidation is common in Fe²⁺ complexes of secondary amine containing macrocycles.¹⁸⁷ As expected, the bond distances between the donor nitrogens are shorter for these Fe³⁺ complexes than for related Fe²⁺ complexes. For example, in the Fe²⁺ complexes of B14N4 and B12N4, the Fe-N(3°) bond distances average 2.27 Å (L = B14N4) and 2.26 Å (L = B12N4). In the present cases the average Fe-N(3°) are 2.24 Å (L = H₂B14N4) and 2.22 Å (L = H₂B12N4). Of course, the secondary amine-Fe³⁺ bond lengths are somewhat shorter: Fe-N(2°) averages 2.15 Å for L = H₂B14N4 and 2.17 Å for L = H₂B12N4. Even more affected by the change in metal oxidation state are the Fe-Cl bond distances, which average as follows: 2.43 Å for Fe(B14N4)Cl₂, 2.41 Å for Fe(B12N4)Cl₂, 2.36 Å for the dimer of H₂B14N4, and 2.35 Å for the dimer of H₂B12N4. The Fe-O bond distances are as expected for dimers of this type,¹⁸² averaging 1.83 Å for the dimer of H₂B14N4 and 1.81 Å for the dimer of H₂B12N4.

Perhaps most interesting is the degree of linearity in the Fe-O-Fe bond angles. For the ligand H₂B12N4 dimer, this angle is 178.9(3)°, an almost completely linear value. In contrast, the Fe-O-Fe angle in the ligand H₂B14N4 dimer is only 144.1(2)°. These values approach the extremes for linearity and nonlinearity, respectively, for μ -oxo bridged iron(III) dimers.¹⁸² A possible rationalization of this observation is that the electronic characteristics of H₂B12N4 are compromised by poor complementarity (its small size). This dimensional relationship compromises the N-Fe-N bond angles, which in turn compromises orbital overlap, leading to an electronic effect.

The trend in the ability of the ligands to enclose the metal ion is unaffected by lack of N-substitution. The ligand H₂B14N4 dimer has an average N_{ax}-M-N_{ax} angle of 161.60°, while this angle averages 147.55° for the ligand H₂B12N4 dimer. The N_{eq}-M-N_{eq} angles average 78.85° and 77.70° for the ligand H₂B14N4 dimer and the ligand H₂B12N4 dimer, respectively.

Electrochemistry. Electrochemical studies were used to compare the monomeric complexes of the unsubstituted and benzyl-substituted ligands H₂B14N4, H₂B12N4, Bn₂B14N4,¹⁶⁷ and Bn₂B12N4 with the methyl-substituted ligand B14N4 and B12N4 complexes whose previous characterization gave promise of oxidative catalytic behavior in aqueous media. The new examples provide the opportunity to see the effect of the N-substituents on the accessibility of higher oxidation states of

Table 21. Electrochemistry of unsubstituted and benzyl-substituted cross-bridged ligand complexes

Complex	Solvent	Redox Couple	E _{1/2} (V)	(E _a -E _c) (mV)
Mn(Me ₂ B14N4)Cl ₂	MeCN	Mn ³⁺ /Mn ²⁺	+0.585	61
		Mn ⁴⁺ /Mn ³⁺	+1.343	65
Mn(Me ₂ B12N4)Cl ₂	MeCN	Mn ³⁺ /Mn ²⁺	+0.466	70
		Mn ⁴⁺ /Mn ³⁺	+1.232	102
Mn(Me ₂ B14N4)Cl ₂	DMF	Mn ³⁺ /Mn ²⁺	+0.522	67
Mn(Bn ₂ B14N4)Cl ₂	DMF	Mn ³⁺ /Mn ²⁺	+0.577	72
Mn(Bn ₂ B12N4)Cl ₂	DMF	Mn ³⁺ /Mn ²⁺	+0.400	65
Mn(H ₂ B14N4)Cl ₂	DMF	Mn ³⁺ /Mn ²⁺	+0.239	79
Mn(H ₂ B12N4)Cl ₂	DMF	Mn ³⁺ /Mn ²⁺	+0.389	280
Fe(Me ₂ B14N4)Cl ₂	MeCN	Fe ³⁺ /Fe ²⁺	+0.110	63
Fe(Me ₂ B12N4)Cl ₂	MeCN	Fe ³⁺ /Fe ²⁺	+0.036	64
Fe(Bn ₂ B14N4)Cl ₂	DMF	Fe ³⁺ /Fe ²⁺	+0.157	85
Fe(Bn ₂ B12N4)Cl ₂	DMF	Fe ³⁺ /Fe ²⁺	+0.071	85
Fe(H ₂ B14N4)Cl ₂	DMF	Fe ³⁺ /Fe ²⁺	-0.113	78
Fe(H ₂ B12N4)Cl ₂	DMF	Fe ³⁺ /Fe ²⁺	-0.055	89

the metal complexes. The cyclic voltammograms of the complexes were obtained in either acetonitrile or DMF in an inert atmosphere glovebox. The redox potentials and peak separations are shown in **Table**

21. These rigid ligands stabilize a range of oxidation states for manganese in acetonitrile, from Mn²⁺ to Mn⁴⁺ as shown by the two reversible oxidations of Mn(B14N4)Cl₂ and Mn(B12N4)Cl₂. In contrast, only the Fe³⁺/Fe²⁺ couple is observed for Fe(B14N4)Cl₂ and Fe(B12N4)Cl₂ in acetonitrile. Unfortunately, the complexes of the unsubstituted and benzyl-substituted ligands are not sufficiently soluble in acetonitrile to permit electrochemical studies in that medium. But, these complexes did have good

solubility in DMF, and cyclic voltammograms of these complexes were obtained in this solvent. The complex $\text{Mn}(\text{B14N4})\text{Cl}_2$ was examined in both solvents as a test for the effect of solvent on the redox potentials. This complex only exhibits one reversible oxidation in DMF, because the solvent itself becomes oxidized, as evidenced by large current jumps, at potentials corresponding to the $\text{Mn}^{4+}/\text{Mn}^{3+}$ couple. The $\text{Mn}^{3+}/\text{Mn}^{2+}$ couple, however is observed in both solvents with only small changes in potential or reversibility (+0.585 V(61mV) in MeCN vs. +0.522 V(67mV) in DMF). There is, as observed before, a significant ring size effect between the 14-membered and the 12-membered ligands. The smaller ring complexes are generally easier to oxidize, which may be explained simply on the basis of size; the smaller cavity more greatly stabilizes the smaller oxidized metal ion. Conversely, the larger ligand favors the larger lower valent metal ion. Only in the unsubstituted ligands $\text{H}_2\text{B14N4}$ and $\text{H}_2\text{B12N4}$ is this trend reversed. With these ligands, in both the Fe^{2+} and Mn^{2+} complexes, the complex of the larger ligand is slightly easier to oxidize. The unsubstituted ligands may be less rigid than the all tertiary N versions, allowing $\text{H}_2\text{B14N4}$ to more easily adapt to the small Fe^{3+} ion than in the cases of the substituted ligands. Ligand $\text{H}_2\text{B12N4}$, because of its small size, should retain more of its rigidity even when unsubstituted, and may not adjust to small Fe^{3+} as well. In spite of the electrochemistry, the overall ability of $\text{H}_2\text{B14N4}$ to engulf Fe^{3+} is still greater than that of $\text{H}_2\text{B12N4}$ (see discussion of dimer crystal structures above).

Finally, there appears to be only a small effect on the redox potentials in going from the methyl-substituted to the benzyl-substituted derivatives. For example the $\text{Mn}^{3+}/\text{Mn}^{2+}$ wave changes only from +0.522 V for $\text{Mn}(\text{B14N4})\text{Cl}_2$ to +0.577 V in $\text{Mn}(\text{Bn}_2\text{B14N4})\text{Cl}_2$. The $\text{Fe}^{3+}/\text{Fe}^{2+}$ wave is similarly changed only from +0.110 V for $\text{Fe}(\text{B14N4})\text{Cl}_2$ to +0.157 V in $\text{Fe}(\text{Bn}_2\text{B14N4})\text{Cl}_2$. Similar effects are observed in the complexes of $\text{H}_2\text{B12N4}$ as compared to those of B12N4 . There is, however a substantial change in redox potentials between the complexes of the methyl-

substituted and the unsubstituted ligands. The $\text{Mn}^{3+}/\text{Mn}^{2+}$ wave changes from +0.522 V for $\text{Mn}(\text{B14N4})\text{Cl}_2$ to +0.239 V in $\text{Mn}(\text{H}_2\text{B14N4})\text{Cl}_2$. The $\text{Fe}^{3+}/\text{Fe}^{2+}$ wave is also significantly changed from +0.110 V for $\text{Fe}(\text{B14N4})\text{Cl}_2$ to -0.113 V in $\text{Fe}(\text{H}_2\text{B14N4})\text{Cl}_2$. But, this effect is lessened in the complexes of $\text{H}_2\text{B12N4}$ and B12N4 , where the $\text{Mn}^{3+}/\text{Mn}^{2+}$ wave changes only from +0.466 V for $\text{Mn}(\text{B12N4})\text{Cl}_2$ to +0.389 V in $\text{Mn}(\text{H}_2\text{B12N4})\text{Cl}_2$. The $\text{Fe}^{3+}/\text{Fe}^{2+}$ wave is changed only from +0.110 V for $\text{Fe}(\text{B12N4})\text{Cl}_2$ to -0.055 V in $\text{Fe}(\text{H}_2\text{B12N4})\text{Cl}_2$. Again, large changes in the flexibility between the substituted and unsubstituted versions of the 14N4 derived complexes might explain why such a large difference in their redox potentials is observed. But the smaller 12N4 derived complexes are still relatively rigid regardless of substitution, and thus the redox potentials are less modified, in the unsubstituted complexes.

In summary, above is reported the synthesis of Mn^{2+} and Fe^{2+} complexes of the unsubstituted and benzyl-substituted cross-bridged macrobicyclic ligands derived from 14N4 and 12N4. The redox potentials of these complexes are not greatly changed from those of the previously characterized complexes of the parent ligands. It is therefore expected that they will not have vastly different aqueous reactivities. The new complexes also suffer the disadvantage of being only sparingly soluble in water. Also, the crystal structures of the two Fe^{3+} complexes of the unsubstituted ligands show that dimerization is possible without the steric interventions of the N-substituents. These factors combine to suggest that further studies on the catalytic behavior of this class of complexes are best reserved for the “parent”, methyl-substituted complexes, until other derivatives of greater solubility and more perturbed electrochemistry are designed and synthesized.